ChemComm

Accepted Manuscript

Volume 52 | Number 1 | 4 January 2016 | Pages 1–216

ChemComm

Chemical Communications
www.rsc.org/chemcomm

ISSN 1359-7345

ROYAL SOCIETY OF CHEMISTRY

COMMUNICATION
Marilyn M. Olmstead, Alan L. Balch, Josep M. Poblet, Luis Echegoyen et al.
Reactivity differences of Sc_xNb_yC_n (2n = 68 and 80). Synthesis of the first methanofullerene derivatives of Sc_3N@C_n

175 YEARS

This is an Accepted Manuscript, which has been through the Royal Society of Chemistry peer review process and has been accepted for publication.

Accepted Manuscripts are published online shortly after acceptance, before technical editing, formatting and proof reading. Using this free service, authors can make their results available to the community, in citable form, before we publish the edited article. We will replace this Accepted Manuscript with the edited and formatted Advance Article as soon as it is available.

You can find more information about Accepted Manuscripts in the author guidelines.

Please note that technical editing may introduce minor changes to the text and/or graphics, which may alter content. The journal's standard Terms & Conditions and the ethical guidelines, outlined in our author and reviewer resource centre, still apply. In no event shall the Royal Society of Chemistry be held responsible for any errors or omissions in this Accepted Manuscript or any consequences arising from the use of any information it contains.

ROYAL SOCIETY OF CHEMISTRY

rsc.li/chemcomm

Journal Name

COMMUNICATION

Design and synthesis of dopant-free organic hole-transport materials for perovskite solar cells

Linqin Wang,[‡a] Jinbao Zhang,[‡b] Peng Liu,[‡c] Bo Xu,[d] Biaobiao Zhang,[a] Hong Chen,[a] A. Ken Inge,[e] Yuanyuan Li,[f] Haoxin Wang,[g] Yi-Bing Cheng,[b] Lars Kloo[c] and Licheng Sun *[ag]

Two novel dopant-free hole-transport materials (HTMs) with spiro[dibenzo[c,h]xanthene-7,9'-fluorene] (SDBXF) skeletons were prepared via facile synthesis routes. A power conversion efficiency of 15.9% in perovskite solar cells is attained by using one HTM without dopants, which is much higher than nondoped Spiro-OMeTAD-based devices (10.8%). The crystal structures of both new HTMs were systematically investigated to reveal the reasons behind such differences in performance and to indicate the design principles of more advanced HTMs.

Perovskite solar cells (PSCs) have attracted great attention during the past years with a certified power conversion efficiency (PCE) up to 22.7%.[1-5] In the PSC devices, novel hole-transport materials (HTMs) play a critical role for the improvement of device performance and stability.[6] The most well-known HTM, Spiro-OMeTAD (2,2',7,7'-tetrakis(N,N'-di-p-methoxyphenylamine)-9,9'-spirobifluorene), was originally reported by Grätzel and co-workers.[7] However, the high cost of the raw materials and the tedious synthetic routes limit its wide application. Besides, organic HTMs typically show relatively low conductivity, and therefore most of the reported HTMs need to be doped with additives, in order to increase the conductivity of the HTM and the PCE of the PSCs.[8-10], The dopants, however,

are commonly hydrophilic, which have been shown to accelerate the degradation of the perovskite crystals and induce device instability. Therefore, the design of novel dopant-free HTMs is necessary for applications in PSCs. Efforts have been devoted to develop new dopant-free HTMs based on different core structures.[11-14] For example, Xu et al. recently designed and synthesized two HTMs based on the indacenodithiophene (IDT) unit with long alkyl chains as substituents.[15] The co-planarity of the IDT units were found to improve intermolecular interactions and most likely promote a higher hole mobility with methoxytriphenylamine (TPA) as the extending units. Sun and Johansson et al. reported a dopant-free HTM including the charged moieties accompanied by counter ions.[16] They found that the new type of ionic HTMs shows higher hole conductivity, and the obtained devices demonstrated better PCE than standard Spiro-OMeTAD-based devices. Jen and Chen et al. presented a new structural HTM, Trux-OMeTAD, consisting of a C_{3h} truxene core with arylamine terminals and hexyl side-chains.[17] The PSCs based on Trux-OMeTAD as HTM showed a high PCE of 18.6% with minimal hysteresis. In addition, excellent hole mobility was exhibited in this planar, rigid and fully conjugated molecule, and suitable energy levels matched those of the perovskite materials.

Recently, several HTMs were reported with a spiro[fluorine-9,9'-xanthene] (SFX) backbone as the core unit.[18-20] In the SFX unit, there is a tetrahedral sp³-hybridized carbon atom between two perpendicular π systems composing a three-dimensional (3D) structural architecture which can reduce both charge recombination and electronic coupling in the HTM layer. In addition, this rigid spiro conjugation is able to enhance the charge-transport ability of hole transfer.[21] Previous work from our group showed that the estimated synthetic cost for the SFX core is 30 times lower than that of the spiro-bi[fluorine] (SBF) core, and a synthesis yield of over 90% can be achieved when phenol and 9-fluorenone are used as raw materials.[10, 22]

One of the more promising strategies to construct dopant-free HTMs for PSCs is based on the introduction of larger π-conjugated systems to the HTM molecules, which have the

a. Organic Chemistry, Department of Chemistry, KTH Royal Institute of Technology, SE-10044 Stockholm, Sweden.
   E-mail: lichengs@kth.se
b. Department of Materials Science and Engineering, 22 Alliance Lane, Monash University, VIC 3800, Australia.
c. Applied Physical Chemistry, Center of Molecular Devices, Department of Chemistry, KTH-Royal Institute of Technology, SE-10044 Stockholm, Sweden.
d. Department of Chemistry, Ångström Laboratory, Box 523, Uppsala University, 75120 Uppsala, Sweden.
e. Department of Material and Environmental Chemistry (MMK), Stockholm University, SE-10691 Stockholm, Sweden.
f. Wallenberg Wood Science Center, Department of Fibre and Polymer Technology, KTH Royal Institute of Technology, SE-100 44 Stockholm, Sweden
g. State Key Laboratory of Fine Chemicals, Institute of Artificial Photosynthesis, DUT-KTH Joint Education and Research Centre on Molecular Devices, Dalian University of Technology, 116024 Dalian, China.

‡ These authors contribute equally to this work.
† Electronic Supplementary Information (ESI) available. See DOI: 10.1039/x0xx00000x

COMMUNICATION

potential to improve the conductivity of the hole transport layers. Herein, two new dopant-free HTMs, $N^{2'},N^{2'},N^{7'},N^{7'}$-tetrakis(4-methoxyphenyl)spiro[dibenzo[*c*,*h*] xanthene-7,9'-fluorene]-2',7'-diamine (X61) and $N^{2'},N^{2'},N^{5},N^{5},N^{7'},N^{7'},N^{9},N^{9}$-octakis(4-methoxyphenyl)spiro [dibenzo[c,h]xanthene-7,9'-fluorene]-2',5,7',9-tetraamine (X62), with spiro[dibenzo[*c*,*h*] xanthene-7,9'-fluorene] (SDBXF) as the skeleton were designed and synthesized. A systematic crystallographic investigation of both HTMs offers more detailed insights into the molecular packing features. The SDBXF skeleton also represents a spiro core but has an extended π conjugation system in comparison to the well-known SFX skeleton. The introduction of the naphthalene group could increase the conjugation system of the HTMs, leading to more efficient π−π stacking in HTM films. This is expected to be beneficial for the charge transport.
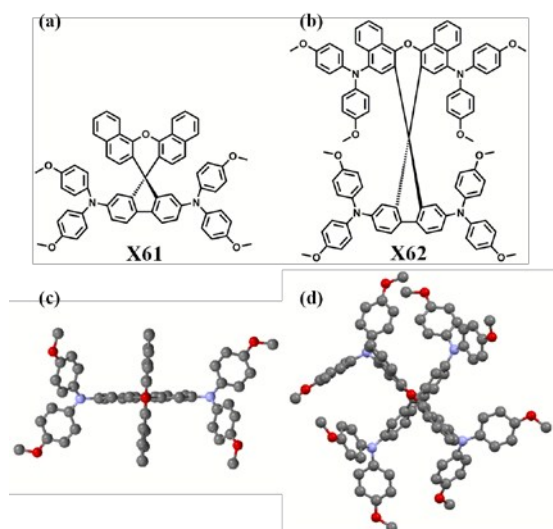

Fig. 1 Molecular structures and single crystal X-ray structures of HTM **X61** (a, c) and **X62** (b, d).

The molecular structures obtained from single crystal X-ray diffraction (SCXRD) of the two HTMs are shown in Fig. 1. In our approach to synthesize the final products **X61** and **X62**, 1-naphthol and 2,7-dibromo-9-fluorenone were used as starting materials, respectively, followed by a simple Buchwald-Hartwig reaction. Detailed experimental procedures of the synthesis is presented in the ESI.† The normalized UV-Visible absorption and photoluminescence spectra of **X61** and **X62** are shown in Fig. S7, and the corresponding data are listed in Table S1. Both **X61** and **X62** display similar maximum absorption peaks around 382 nm. Their narrow absorption spectra below 430 nm are favourable for minimizing parasitic absorption from the HTM layer for the utilization in perovskite tandem solar cell devices. The emission peaks of **X61** and **X62** at 432 nm and 483 nm, respectively, indicate that the dimethoxydiphenylamine units induce only small effects on the absorption property but apparently affect the emission property. The optical band gap E_{0-0} of the HTMs can be obtained from the intersection of the absorption and emission spectra, which are shown in Table S1. In order to investigate their redox properties, the oxidation potentials of both HTMs were also studied by cyclic

voltammetry (CV) and differential pulsed voltammetry (DPV) (Fig. S8 and S9 respectively) in DCM solution with a concentration of 10^{-4} M, and the corresponding data are listed in Table S1. The highest occupied molecular orbital (HOMO) energy levels of the HTMs were determined by the above procedure. Both HTMs show a similar HOMO energy level (−5.11 eV for **X61**, and −5.14 eV for **X62**) as that of Spiro-OMeTAD (−5.10 eV). This indicates that both molecules are suitable for hole transfer processes from the perovskite layer to the HTM films, and match the work function of the Au counter electrode. For the lowest unoccupied molecular orbital (LUMO) energy levels, as shown in Fig. 2a, both HTMs have much higher LUMO energy levels (−2.09 eV and −2.22 eV for **X61** and **X62**, respectively) than the conduction band (CB) of the perovskite, suggesting that the transfer of the photogenerated electrons from the perovskite layer to the Au counter electrode material is effectively suppressed. For a better understanding of the energy levels and the electronic distribution in the molecular building blocks in both HTMs, density functional theory (DFT) calculations were performed at B3LYP/6-31G(d) level with the Gaussian 09 program (see Fig. S10). The HOMOs of both molecules are delocalized in the bottom fluorene and dimethoxydiphenylamine units, while the LUMOs of these molecules are mainly delocalized in the dibenzo-xanthene moieties. The spatially separated HOMOs and LOMOs could forecast good hole transporting properties.
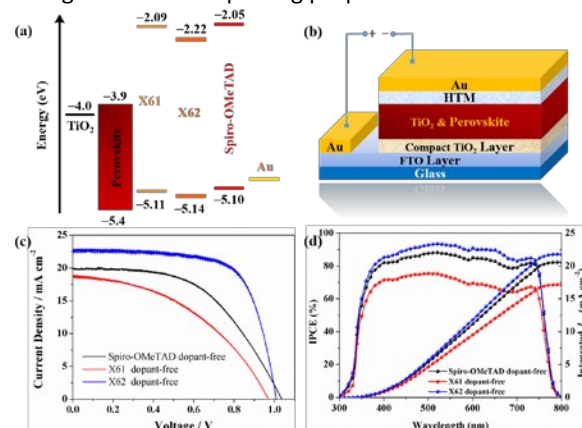

Fig. 2 (a) Energy level diagram; (b) sketch map of the PSCs; (c) *J-V* characteristics of **X61**, **X62**, and Spiro-OMeTAD based PSCs measured under 100 mW cm^{-2} AM1.5G; (d) Corresponding IPCE spectra and integrated J_{SC} of the devices.

As mentioned before, charge transport is a significant factor to consider in the design of highly efficient HTMs for PSCs. Both the hole mobility and conductivity are critical factors for determining the potential eligibility of new HTMs in PSCs, since they can significantly influence the hole collection efficiency in the devices. In this work, we used two-probe electrical conductivity measurements to investigate the conductivities of the HTMs and the space charge limited current (SCLC) method to determine the hole mobility. The obtained *J-V* curves are shown in Figures S11 and S12, and corresponding data are estimated as shown in Table S2. The HTM solutions used for film formation in the above measurements were the same as when

ChemComm

Journal Name

COMMUNICATION

manufacturing the solar cell devices without dopants, and all details can be found in the ESI.† Under such conditions, **X62** shows a higher conductivity (5.14×10^{-6} S·cm^{-1}) than **X61** (3.98×10^{-6} S·cm^{-1}) and Spiro-OMeTAD (4.56×10^{-6} S·cm^{-1}). This may be due to **X62** having a larger conjugated system and structural extension, resulting in more efficient $\pi-\pi$ stacking in the hole transporting films. In addition, **X62** also exhibits a higher hole mobility (7.95×10^{-5} cm^2·V^{-1}·s^{-1}) than that of **X61** (3.91×10^{-5} cm^2·V^{-1}·s^{-1}) and Spiro-OMeTAD (6.06×10^{-5} cm^2·V^{-1}·s^{-1}).

Table 1 Photovoltaic parameters of the devices based on the dopant-free HTMs **X61**, **X62** and Spiro-OMeTAD.

HTMs	J_{SC} (mA·cm^{-2})	J_{SC} Cal. (mA·cm^{-2})	V_{OC} (V)	FF (%)	PCE (%)
X61	18.6	17.2	0.97	44.1	8.0
X62	22.4	21.9	1.01	70.4	15.9
Spiro-OMeTAD	19.9	20.6	1.04	52.6	10.8

The PSC devices were fabricated with the standard structure of FTO/TiO$_2$ compact layer/Meso-TiO$_2$/Mixed-perovskite/HTM/Au. The concentration of the HTM solutions used for film formation by spin coating in the devices was optimized to 18 mg/mL. In addition, the HTM coverage on the top of the perovskite layer were investigated by scanning electron microscopy (SEM) (Figure S13), from which we noted that the perovskite crystal was fully covered by the HTM materials when the solution concentration exceeds 15 mg/mL. Obviously, X62 shows better film-forming ability that can effectively to supress charge recombination between the perovskite and the HTM, which is coherent with the recombination resistance (R$_{rec}$) obtained from electrochemical impedance spectroscopy (EIS, Figure S21 and Table S4). Figure 2c shows the J-V curves of the PSCs based on different HTMs and the corresponding parameters are given in Table 1. Under optimal conditions, the **X62**-based PSCs showed the best performance with a PCE of 15.9%, a short-circuit photocurrent density (J_{SC}) of 22.4 mA·cm^{-2}, an open-circuit photovoltage (V_{OC}) of 1.01 V, and a fill factor (FF) of 70.4%. In contrast, the **X61**-based PSC devices yielded a lower PCE of 8.0%, with a J_{SC} of 18.6 mA·cm^{-2}, a V_{OC} of 0.97 V, and an FF of 44.1%. As a reference, devices based on the standard HTM Spiro-OMeTAD under the same conditions showed an efficiency of 10.8%, with a J_{SC} of 19.9 mA·cm^{-2}, a V_{OC} of 1.04 V and an FF of 52.6%. Figure 2d shows the incident photon-to-current-conversion efficiency (IPCE) spectra and the corresponding integrated J_{SC} of the PSC devices with **X61**, **X62** and Spiro-OMeTAD. The **X62**-based PSC devices show much higher IPCE values than both those based on **X61** and Spiro-OMeTAD. The calculated photocurrents from the IPCE spectra agree well with the J_{sc} obtained from the J-V experiments.

Among these devices, **X62**-based PSCs reached the highest J_{SC}, which might be due to a higher charge collection efficiency ascribed to the higher hole mobility and conductivity. As a comparison, the lower hole conductivity of **X61** and Spiro-OMeTAD results in a higher series resistance in the devices, which is in good agreement with the series resistance (Rs) determined by EIS and shown in Figure S21 and Table S4. Besides, the higher resistance of the **X61** and Spiro-OMeTAD films leads to lower FF in the PSC devices. However, the V_{OC} of both **X61** and **X62** based devices are lower than for Spiro-OMeTAD-based PSCs, probably due to a higher recombination

loss in the two new materials. The device stability was investigated in ambient conditions at room temperature with a relative humidity of about 50%. After 10 days, the efficiencies of the non-doped Spiro-OMeTAD, X61 and X62 based solar cells retained 81%, 49% and 80% of the initial efficiency, respectively (Figure S20). This result demonstrates that dopant-free HTMs play a critical role in the long-term stability of the PSCs. The enhanced device stability of X62 is another promising property for its future application in PSCs.

In order to further investigate the photovoltaic properties of the PSCs based on **X61** and **X62**, the hole transfer kinetics at the perovskite/HTM interface were characterized by steady-state photoluminescence and time-resolved fluorescence decay (Fig. S14). The charge transfer occurs at the perovskite/HTM interface is shown in Fig. S14a. The pristine perovskite film shows a long-lived decay with a half time constant of 85 ns, while the perovskite films capped by the HTMs exhibit a much shorter time constant. The **X61** coated perovskite film shows a half time constant of 7.6 ns. In comparison, the **X62** coated one exhibits the shortest half time constant of 7.1 ns. This indicates that **X62** mediates a faster hole-transport process, which agree well with the higher J_{SC} obtained from the **X62**-based PSCs.

In order to attain further insights into the charge transport of these two SDBXF skeleton based HTMs, single crystals of **X61** and **X62** were grown by liquid diffusion method from organic solvents. The crystal structure of **X61** (triclinic, space group: P-1) and **X62** (monoclinic, space group: P2$_1$/c) have been determined by single crystal X-ray diffraction (SCXRD) analysis, as shown in Fig. S15, and perspective views along different unit cell axes are illustrated in Fig. S16.
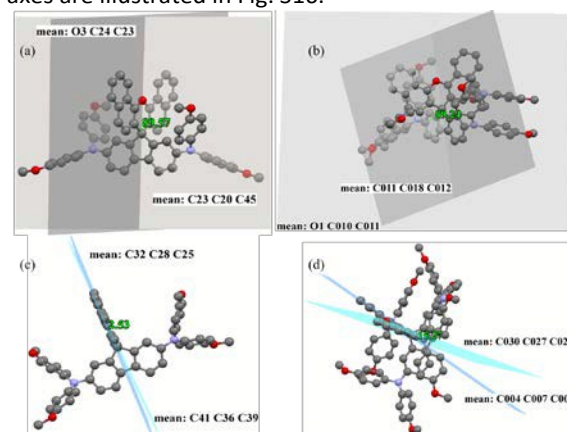

Fig. 3 Dihedral angle of **X61** (a, c) and **X62** (b, d) obtained from SCXRD. The light grey, dark grey, light blue and dark blue colored planes represent the dibenzo[c,h]xanthene unit, fluorene unit and two naphthalene units, respectively. Hydrogen atoms are omitted for clarity.

The dihedral angle between the dibenzo[c,h]xanthene (DBX) unit and the fluorene unit are 89.6° and 89.2°, respectively, for **X61** and **X62** (see Fig. 3a and 3b), which are similar to that in Spiro-OMeTAD (89.9°).[23] These dihedral angles indicate weak intermolecular interaction with minimal molecular stacking which benefit the formation of amorphous solid.[24] The angles between the two close naphthalene units next to the non-aromatic central ring are 2.5° and 15.3°, respectively, for **X61**

COMMUNICATION

and **X62** (see Fig. 3c and 3d), which may weaken the $\pi-\pi$ interaction between any two DBX units preventing dense packing and aggregation. The crystal packing details of **X61** and **X62** are provided in Fig. S17.

In **X61** (Fig. 4a), the shortest $\pi-\pi$ contact between the DBX unit and the dimethoxyphenylamine moieties is 3.216 Å, while the interaction distances are 2.808 Å and 2.659 Å for CH/π interactions and O-H hydrogen bonds, respectively. As for **X62** (Fig. 4b), when observed perpendicular to ac plane (i.e. view along b axis), each molecule has multiple short contacts with surrounding molecules, including O-H, CH/π hydrogen bonds, C-O, and $\pi-\pi$ short contacts with the shortest interaction distances of 2.567 Å, 2.882 Å, 3.112 Å and 3.313 Å. The large abundance of short contacts between the **X62** molecules could provide sufficient channels for efficient charge transport and result in better photovoltaic performance. Therefore, incorporation of suitable substituents on the dibenzo[c,h]xanthene skeleton is of great importance for 3D spatial extension in molecular stacking and for enhancing the charge transporting properties of new HTMs.
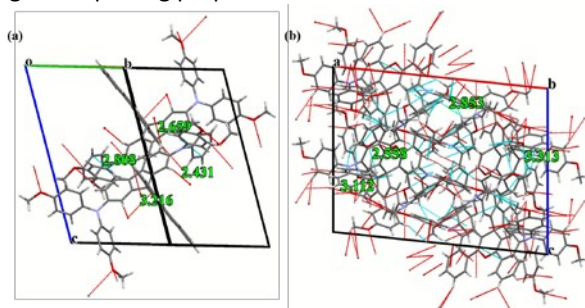

Fig. 4 O-H, CH/π hydrogen bonds, C-O, and $\pi-\pi$ short contacts observed in the packing of **X61** (a) and **X62** (b) crystals obtained from SCXRD.

In summary, we have successfully designed and synthesized two new spiro-type HTMs, named **X61** and **X62**, with SDBXF as the skeleton. X-ray crystallographic analysis of the single crystals of both HTMs was carried out in this study, in which multiple short contacts are found beneficial for the enhancement of charge transfer. The corresponding dopant-free PSCs based on **X62** exhibit a maximum efficiency of 15.96% (working area, 0.16 cm^2), which outperform the standard Spiro-OMeTAD based devices (10.84%). A higher IPCE shown by devices based on **X62** is consistent with the high J_{SC} of 22.42 mA·cm^{-2}. Our study highlights the potential application of SDBXF-skeleton-based molecules as dopant-free HTMs for high performance PSCs.

Conflicts of interest

There are no conflicts to declare.

References

1. M. M. Lee, J. Teuscher, T. Miyasaka, T. N. Murakami and H. J. Snaith, *Science*, 2012, **338**, 643-647.
2. M. Liu, M. B. Johnston and H. J. Snaith, *Nature*, 2013, **501**, 395-398.
3. D. Bi, W. Tress, M. I. Dar, P. Gao, J. Luo, C. Renevier, K. Schenk, A. Abate, F. Giordano, J. P. Correa Baena, J. D. Decoppet, S. M. Zakeeruddin, M. K. Nazeeruddin, M. Gratzel and A. Hagfeldt, *Sci Adv*, 2016, **2**, e1501170.
4. M. Saliba, T. Matsui, K. Domanski, J. Y. Seo, A. Ummadisingu, S. M. Zakeeruddin, J. P. Correa-Baena, W. R. Tress, A. Abate, A. Hagfeldt and M. Gratzel, *Science*, 2016, **354**, 206-209.
5. https://www.nrel.gov/pv/assets/ images/efficiency-chart.png.
6. L. Calio, S. Kazim, M. Gratzel and S. Ahmad, *Angew Chem Int Ed Engl*, 2016, **55**, 14522-14545.
7. M. Grätzel, U. Bach, D. Lupo, P. Comte, J. E. Moser, F. Weissörtel, J. Salbeck and H. Spreitzer, *Nature*, 1998, **395**, 583-585.
8. J. Zhang, Y. Hua, B. Xu, L. Yang, P. Liu, M. B. Johansson, N. Vlachopoulos, L. Kloo, G. Boschloo, E. M. J. Johansson, L. Sun and A. Hagfeldt, *Advanced Energy Materials*, 2016, **6**, 1601062.
9. W. H. Nguyen, C. D. Bailie, E. L. Unger and M. D. McGehee, *J Am Chem Soc*, 2014, **136**, 10996-11001.
10. B. Xu, J. Zhang, Y. Hua, P. Liu, L. Wang, C. Ruan, Y. Li, G. Boschloo, E. M. J. Johansson, L. Kloo, A. Hagfeldt, A. K. Y. Jen and L. Sun, *Chem*, 2017, **2**, 676-687.
11. W. S. Yang, B. W. Park, E. H. Jung, N. J. Jeon, Y. C. Kim, D. U. Lee, S. S. Shin, J. Seo, E. K. Kim, J. H. Noh and S. I. Seok, *Science*, 2017, **356**, 1376-1379.
12. G.-W. Kim, G. Kang, J. Kim, G.-Y. Lee, H. I. Kim, L. Pyeon, J. Lee and T. Park, *Energy & Environmental Science*, 2016, **9**, 2326-2333.
13. J. Liu, Y. Wu, C. Qin, X. Yang, T. Yasuda, A. Islam, K. Zhang, W. Peng, W. Chen and L. Han, *Energy Environ. Sci.*, 2014, **7**, 2963-2967.
14. H.-C. Liao, T. L. D. Tam, P. Guo, Y. Wu, E. F. Manley, W. Huang, N. Zhou, C. M. M. Soe, B. Wang, M. R. Wasielewski, L. X. Chen, M. G. Kanatzidis, A. Facchetti, R. P. H. Chang and T. J. Marks, *Advanced Energy Materials*, 2016, **6**, 1600502.
15. X. Liu, E. Rezaee, H. Shan, J. Xu, Y. Zhang, Y. Feng, J. Dai, Z.-K. Chen, W. Huang and Z.-X. Xu, *Journal of Materials Chemistry C*, 2018, **6**, 4706-4713.
16. J. Zhang, B. Xu, L. Yang, A. Mingorance, C. Ruan, Y. Hua, L. Wang, N. Vlachopoulos, M. Lira-Cantú, G. Boschloo, A. Hagfeldt, L. Sun and E. M. J. Johansson, *Advanced Energy Materials*, 2017, **7**, 1602736.
17. C. Huang, W. Fu, C. Z. Li, Z. Zhang, W. Qiu, M. Shi, P. Heremans, A. K. Jen and H. Chen, *J Am Chem Soc*, 2016, **138**, 2528-2531.
18. B. Xu, Z. Zhu, J. Zhang, H. Liu, C.-C. Chueh, X. Li and A. K. Y. Jen, *Advanced Energy Materials*, 2017, **7**, 1700683.
19. G. Kadam, A. Anuradha, A. Agarwal, A. Puyad, D. D. La, R. A. Evans, J. Li, A. Gupta and S. V. Bhosale, *Materials Chemistry Frontiers*, 2018, DOI: 10.1039/c8qm00067k.
20. M. Maciejczyk, A. Ivaturi and N. Robertson, *Journal of Materials Chemistry A*, 2016, **4**, 4855-4863.
21. V. Govindan, K.-C. Yang, Y.-S. Fu and C.-G. Wu, *New Journal of Chemistry*, 2018, **42**, 7332-7339.
22. B. Xu, D. Bi, Y. Hua, P. Liu, M. Cheng, M. Grätzel, L. Kloo, A. Hagfeldt and L. Sun, *Energy & Environmental Science*, 2016, **9**, 873-877.
23. P. Ganesan, K. Fu, P. Gao, I. Raabe, K. Schenk, R. Scopelliti, J. Luo, L. H. Wong, M. Grätzel and M. K. Nazeeruddin, *Energy & Environmental Science*, 2015, **8**, 1986-1991.
24. D. Bi, B. Xu, P. Gao, L. Sun, M. Grätzel and A. Hagfeldt, *Nano Energy*, 2016, **23**, 138-144.